SEMARAK ILMU PUBLISHING

Journal of Advanced Research in Applied Sciences and Engineering Technology

Journal homepage:
https://semarakilmu.com.my/journals/index.php/applied_sciences_eng_tech/index
ISSN: 2462-1943

Performance Analysis of Strain Sensor Based on Fiber Bragg Grating

Nurul Farhana Husna Kamarozaman[1], Nani fadzlina Naim[1,*], Azita Laily Yusof[1], Norsuzila Ya'cob[1], Suzi Seroja Sarnin[1], Harry Ramza[2]

[1] School of Electrical Engineering, College of Engineering, Universiti Teknologi MARA (UiTM), 40450 Shah Alam, Selangor, Malaysia
[2] Department of Electrical Engineering, Faculty of Industrial and Informatics Technology, Universitas Muhammadiyah Prof. Dr. Hamka, Jalan Tanah Merdeka No.6, KP Rambutan, Jakarta, Indonesia

ARTICLE INFO

Article history:
Received 22 June 2023
Received in revised form 14 January 2024
Accepted 20 June 2024
Available online 10 August 2024

Keywords:
Fiber Bragg grating; strain sensor; sensitivity; Bragg wavelength

ABSTRACT

This project presents on the analysis of strain sensing performance through software simulation and experimental setup. The bare and FBG strain sensors are tested by applying strain at the grating region of the FBG and the output of the experiment is displayed on the optical spectrum analyzer (OSA) in terms of power (dBm) and wavelength (nm). The performance of the FBGs has been evaluated by comparing the strain sensitivity and wavelength shift obtained. The FBG strain sensor has a strain sensitivity of 38.25 pm/N, which is higher than the bare FBG's strain sensitivity of 12.49 pm/N. The FBG strain sensor's experimental and simulation performance is also investigated. OptiSystem software is used to simulate the strain sensor performance. The overall results indicate the ability of FBG to be utilized as a strain sensor as the Bragg wavelength is shifted by the combination effect of effective refractive index and grating period influenced by the changes of strain.

1. Introduction

Fiber Bragg grating (FBG) is a hidden reflector in the core fiber that is tuned to one wavelength of light and transmits all others. To block specific wavelengths, FBG can be employed as an inline optical filter. The first approach by Dr. Kenneth O. Hill and his co-workers paved the way for a number of advancements and innovations in the fabrication of FBGs by Tao *et al*., [1]. FBG is the most mature grating-based sensor, and it is already widely used owing to its advantages. The features include tolerance to electromagnetic interference, resistance to severe conditions and small size. These strengths have resulted in the rapid development and deployment of FBG, particularly in measuring and monitoring devices in a variety of industries.

The refractive index of the optical fiber core area is periodically modulated using an FBG. The FBG has the ability to reflect some emission wavelengths while transmitting others. This assertion is verified by Figure 1, which depicts the operation of the FBG sensor. The spectrum exhibits broad emission when light is launched from the input side of the fiber, as shown in Figure 1(a). However,

* *Corresponding author.*
E-mail address: nanifadzlina@uitm.edu.my

https://doi.org/10.37934/araset.50.1.3446

as illustrated in Figure 1 when light passes through the FBG, only wavelengths that fulfil the Bragg condition are reflected back in the same core (b). In Figure 1(c), the remaining light is transmitted without loss as shown in Aizzuddin *et al*., [2].

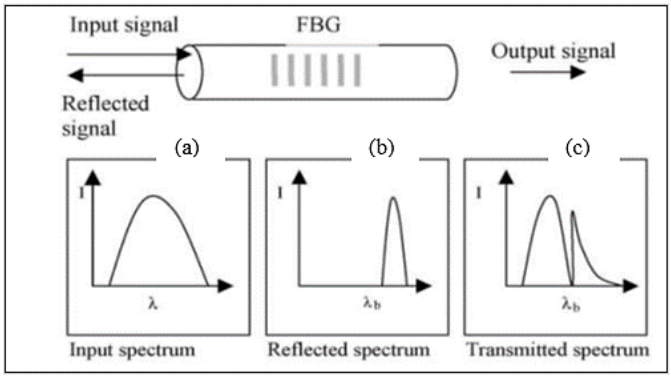

Fig. 1. Transmitted and reflected spectrum from FBG [2]

Bragg wavelength has a narrow spectrum output that reflected from the FBG sensor after being irradiated by the light source. The ability to maintain the grating wavelength is a key characteristic of FBG. FBG reflects light with a characteristic spectrum centered at λ_B , the Bragg wavelength, which is the most essential parameter of an FBG-based sensor because it shifts with strain and temperature variations as stated in Dante *et al*., [3]. The Bragg wavelength, can be written as:

$$\lambda_B = 2n_{eff}\,\Lambda \tag{1}$$

where n_{eff} is the effective refractive index of the fiber's core and is the grating period. As the reflected Bragg wavelength is subject to physical changes, changes in the effective refractive index or grating period will naturally modify it. The maximum wavelength reflectance is affected not only by the Bragg grating, but also by strain and temperature.

The evaluation of maximum wavelength shift caused by the enacted strain is the basic operation of FBG strain sensor. Strain optic effect leads to a variation in both grating period and effective relative index which resulting the Bragg wavelength to be shifted. The measurement of Bragg wavelength shift due to the added strain can be expressed by:

$$\Delta\lambda_B = [(1 - \rho)\,\lambda_B \varepsilon] \tag{2}$$

where ρe is the photoelastic coefficient and ε is the axial strain undergo by the fiber. Compared to the regular electrical strain gauge, FBG strain sensors have more advantages and basically the best strain sensors available as stated in More *et al*., [4].

In this project, the focus is to construct a strain sensing experiment between bare and FBG strain sensors in order to evaluate the performance of the FBGs by comparing the strain sensitivity obtained. Next, both experimental results will be analyzed along with outcomes produced from the simulation process using the OptiSystem Software.

2. Literature Review

During the last decade, many optical fibers sensing have been developed. Optical fiber Bragg grating (FBG) is the most popular among the available sensing techniques. There are various types of FBG sensors that are commonly used in the industry especially strain sensors.

In the work reported by Almubaied *et al*., [5], FBG strain sensor was employed to observe the corrosion of reinforced concrete. A bare FBG sensor was bonded on the structure of steel reinforcement in order to monitor the percentage of corrosion based on the Bragg wavelength shift. From the result obtained, it is displayed that the wavelength shift increases caused by the stress that introduced by the existence of the corrosion. This shows that the FBG strain sensor was strong and sensitive enough to detect the progression of steel bar corrosion in concrete. This early detection of corrosion cracks can reduce the cost for the maintenance and repair of the concrete infrastructure.

In paper Liu *et al*., [6], the writers focused on investigating the slope monitoring resulting from the frequently landslides and other geological disasters occurrences which often cause high financial and humanitarian cost. The wavelength shift increases caused by the stress that introduced by the existence of the corrosion. They have designed a FBG strain sensor that combines the test time, initial measurement accuracy, maximum sliding distance, dynamic range, and remote real-time monitoring, resulting in a better landslide early-warning monitoring system.

An all-fiber sensing system made of gold-plated FBGs and acrylic FBGs that could monitor axial strain and temperature simultaneously was suggested and built in Wu *et al*., [7]. The strain and ambient temperature applied to the sensor were easily monitored by using a spectrometer to detect the shift in the transmission spectrum in real time. As axial strain increased, the entire transmission spectrum shifted towards the long wavelength direction, and the reflection spectrum shifted by acrylate-plated FBG1 and gold-plated FBG2 were same, so the reflection peak did not split. The wavelength shift and strain change obtained from the work indicated a good linear relationship as plotted in Figure 2 below.

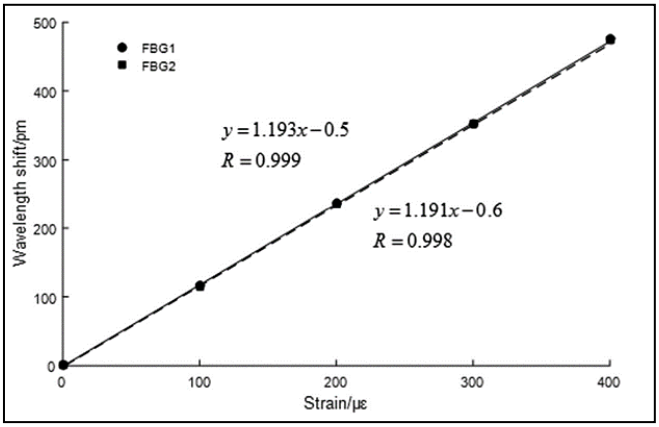

Fig. 2. Wavelength shift in respect to strain changes [7]

While [8, 9] focused on improving the FBG by splicing a handmade twin-core photonic crystal fiber (TCPCF) with two SMF segments and then tapering at each splice site and also by affixing the FBG to a substrate via a lever mechanism. In comparison to the bare FBG result, both works demonstrated that the proposed idea significantly improves strain sensitivity. Due to its great strain sensitivity, the proposed sensors had a wide range of applications in rough industrial environments, particularly mechanical engineering and health monitoring.

Apart from experimental analysis, previous work by Kachare *et al*., Razi *et al*., and Kumar *et al*., [10-13] utilized two friendly user simulation software packages, OptiGrating 4.2.2 and OptiSystem 12, to analyze various FBG combinations. This tool provided a wide range of optical and wireless components enabling the researcher to plan and construct a comprehensive optical network, which was a low-cost, time-saving, and efficient solution. FBG parameters, such as bandwidth, side lobes, peak power, and sensitivity were considered while constructing the FBGs. The OptiGrating 4.2.2 was

used to create various gratings such as uniform, apodized, tilted, and superstructure Figure 3 displays the block diagram designed in OptiSystem [10]. From the result obtained, it could be concluded that the FBGs had a good response towards temperature and strain changes that were applied to it.

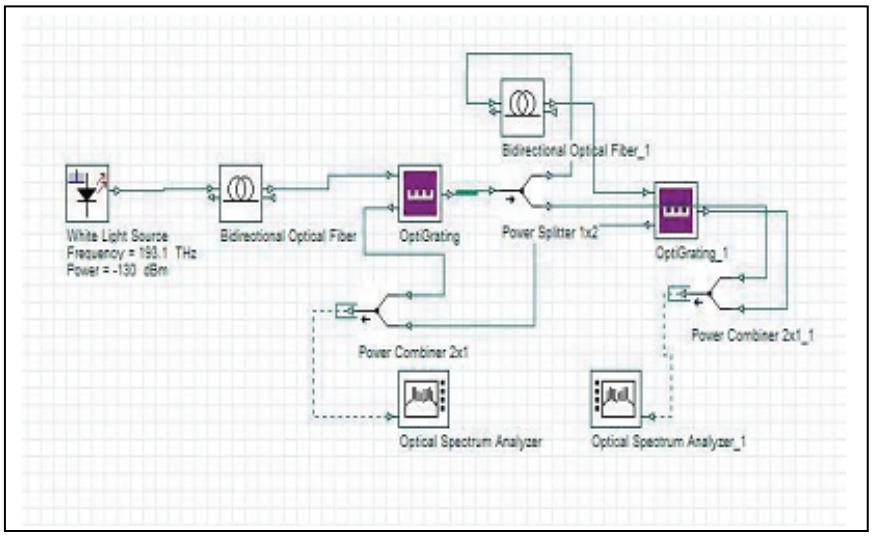

Fig. 3. Block diagram in OptiSystem [10]

Researchers in Elgaud *et al*., [14] also proposed a remote FBG based strain-temperature sensor setup by using a combination of the two modelling tools offered by Optiwave Systems. At varying temperatures, a good linearity between the wavelength shift and strain was found with the same slope for all values, indicating continuous sensitivity throughout the observations. The strain and temperature sensitivity of the two FBGs were determined to be 1.2 pm/strain and 14.4 pm/°C, respectively.

Researchers in [15] have also conducted water leakage detection and localization in tunnels whereas an ultra-weak fiber Bragg grating (UFBG) technology is used as strain sensor. Water leakage is a hazard in tunnel construction which is affected by the underground water as stated in Huang *et al*., Li *et al*., and Yuan *et al*., [16-18]. This leakage will degrade the structure of the tunnel and the surrounding area in terms of safety and strength as mentioned in Wongsaroj *et al*., and Yu *et al*., [19, 20].

3. Research Methodology

3.1 Designing FBG Strain Sensor using Simulation Software

The simulation setup is divided into two components. First, the FBG sensor is constructed and tested using OptiGrating under various strain values for characterization purposes. The created FBG is then exported as spectrum files that OptiSystem can read, allowing it to be deployed later in the sensor setup designed by the OptiSystem tool. The system is then evaluated in terms of its ability to analyze the strain readings based on wavelength shifts caused by strain effect.

3.1.1 OptiGrating section

OptiGrating is used to create consistent FBG sensor with a length of 6 mm, and a modulation index of 0.0001 and the further details of the parameters are as defined in Table 1 with reference to the works by Wu *et al*., [7].

Table 1
Parameters of uniform FBG

Parameters	Details
Core Width (μm)	5
Core Reflective Index	1.46
Cladding Width (μm)	125
Cladding Reflective Index	1.45
Length (mm)	20
Modulation Index	0.0001
Number of segments	25
Center Wavelength (nm)	1539.0067

First, the reflective index and the width of core and cladding need to be determined. Apart from that, all the values shall remain constant. The linearity response and sensitivity to the applied physical measurand of both developed FBG sensors are evaluated. The FBG, centered at 1539.0067 nm, is dedicated to strain changes with constant temperature. Shift in wavelength individually by strain is calculated by the formula given below:

$$\Delta\lambda_B = \lambda_{B\,\text{new}} - \lambda_{B\,\text{original}} \quad (3)$$

where, Δ is the wavelength shift only due to strain, new is the Bragg wavelength obtain when the strain is applied and original is the original Bragg wavelength.

3.1.2 OptiSystem section

The design of a remote sensing optical communication network is simulated in the OptiSystem section. It includes a white light source with a power of -130 dBm, an optical circulator, a single mode fiber of 0.5 km length, FBG sensor designed in OptiGrating that are incorporated as a spectrum file, and an OSA, as shown in Figure 4. Other than that, all parameter in the OptiSystem were using default setting. The strain is then applied by entering the value into the micro-strain box, where the strain changes based on the weight calculation. Also, the temperature remains constant at 25°C. Then, select the spectrum graph option to obtain the result in terms of wavelength (m) vs power (dBm). A light source with a wavelength of 1539.0067 nm is launched into one of the fiber's ends. This signal is sent through the optical circulator. The FBGs reflect some signal at a specific wavelength, which is then directed to the spectrum analyzer through the circulator. The reflected signals are monitored at the OSA, and the specific cause of wavelength shifts is determined.

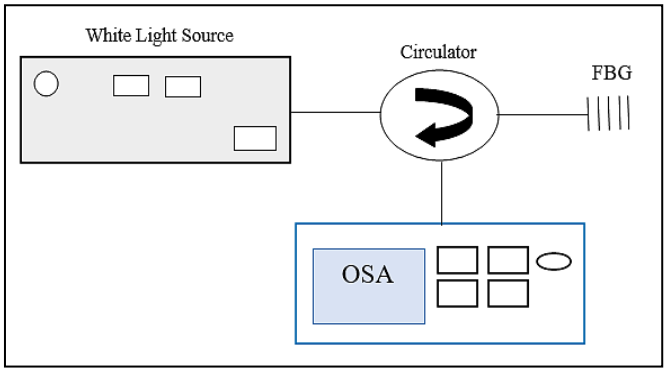

Fig. 4. Schematic diagram of OptiSystem design

3.2. Experimental Setup

Characterization of the spectrum is a must in order to compare the spectrum of the FBG before applying strain variations. For this experiment, the broadband amplified spontaneous emission (ASE) spectrum was use as the broadband light source. YOKOGAWA AQ6370B optical spectrum analyzer (OSA) was utilized to measure and display the output spectrum of the experiment with resolution of 0.2 nm and sampling point of 5000. Figure 5 shows two setups of the characterization of FBG which (a) is for the characterization of transmitted spectrums while (b) is for the FBG reflected spectrum. A circulator is needed in characterizing the reflected spectrum as it allows light to travel in only one direction and managed to get the reflected spectrum to be measured by OSA.

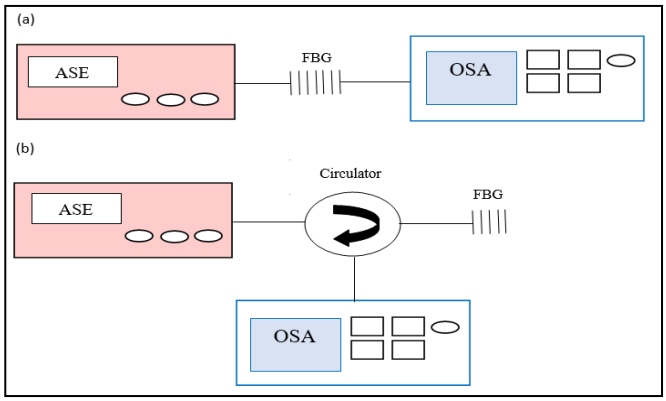

Fig. 5. Schematic diagram of the experiment setup for a) transmitted spectrum of FBG and b) reflected spectrum of FBG

The arrangement of the stain sensor experiment is carried out as in Figure 6. This setup consists of ASE as the broadband light source, OSA to measure the output spectrum, circulator, iron slotted weight with hanger, tripod, clamp and most important thing is the samples of bare and built-in strain sensor FBG. The ASE is connected to port 1 of the circulator while the OSA is connected to the port 3 of the circulator with resolution of 0.2 nm, span of 100.0 nm and sampling point of 5001. The port 2 of the circulator is linked to the end of the FBG.

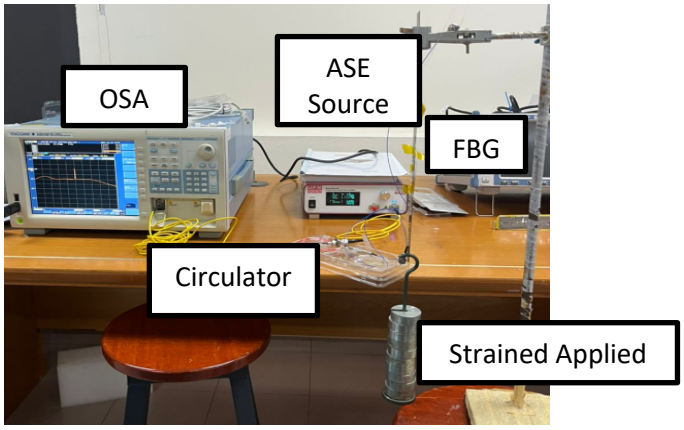

Fig. 6. Experimental setup for strain sensing

The FBG strain sensor is tested against the bare FBG in this experiment to evaluate the performance of the fiber against the applied strain. The fibers are tested in a regular room environment with varied load ranges ranging from 1 N to 10 N. To avoid any instability, the weight

was progressively increased at 10 N increments and maintained for roughly 5 minutes before the data was collected. The OSA data on reflected spectrum is examined and recorded at each desired weight. OSA will display the FBG response in terms of power (dBm) and wavelength (nm). The graph is then saved by selecting the save button and the data is saved as excel documents and graphic form. The wavelength shift can be observed by OSA as the weight is increased. Furthermore, the experiment results can be used to compute and compare the strain sensitivity, linearity, and resolution of the two fibers

4. Result and Discussion

4.1. Analysis of FBG Characterization

Both the ASE spectrum and the bare FBG have been characterised by observing and measuring the output spectrum at the OSA. As mentioned in earlier, the configuration of the end result is shown in Figure 7. The transmission of the ASE spectrum represents the broadband input spectrum. On the other hand, the transmitted spectrum of FBG indicates that the Bragg wavelength has transmitted the light through the fiber core as the wavelength of the light does not fulfil Bragg's condition. The central wavelength of the bare FBG transmission spectrum is at 1544.4910 nm.

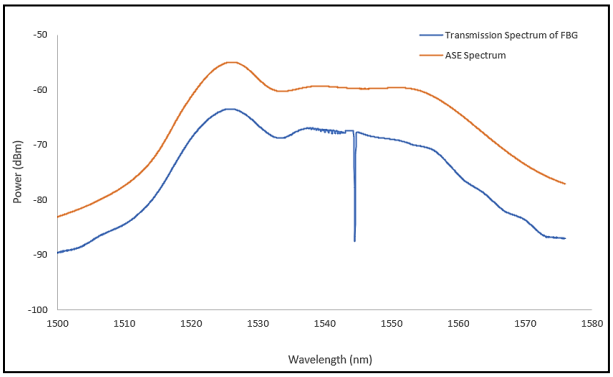

Fig. 7. ASE spectrum and FBG transmitted spectrum

Next, the characterization of FBG involving measuring the signal at which is reflected back through the fiber and enters the circulator port 3 has been carried out. The output of the characterization is measured using OSA. The reflected spectrum is obtained as the wavelength of the input light satisfies the Bragg condition. Figure 8 illustrates the reflected spectrum of the bare FBG and the central wavelength of the FBG reflected spectrum is at $\Delta\lambda_B$=1544.4910 nm while the center of Bragg wavelength for the built-in FBG strain sensor is at 1539.0067 nm as in Figure 9. The power recorded in these characterizations are lower compared to the transmission characterization due to the use of a circulator, which generates losses.

Following that, OptiGrating simulation was also used to study the characteristics of the FBG strain sensor. The reflection and transmission spectra are displayed in Figure 10. It demonstrates that the spectrum matches those provided by the OptiGrating samples library. The proposed FBG sensor were evaluated in terms of their linearity responsiveness and sensitivity to physical stimuli measurand.

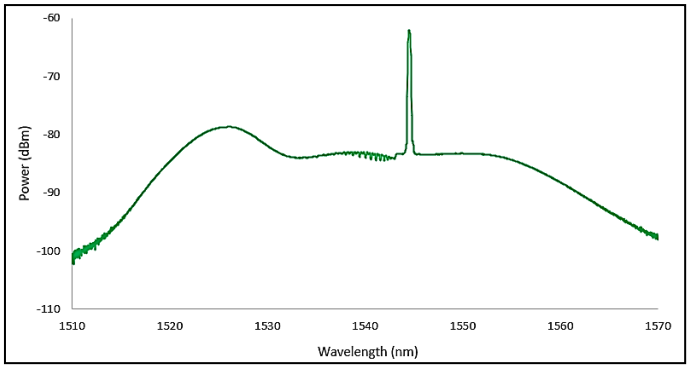

Fig. 8. Reflected spectrum of bare FBG

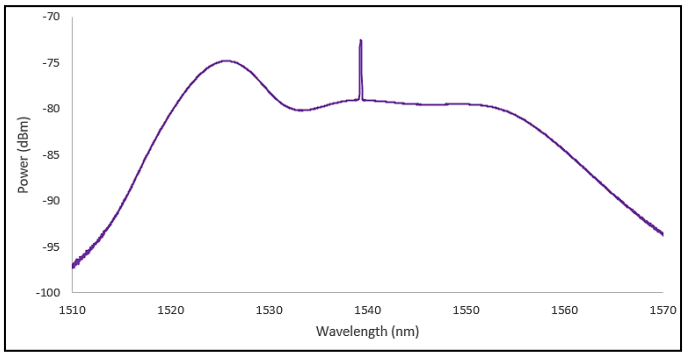

Fig. 9. Reflected spectrum of FBG strain sensor

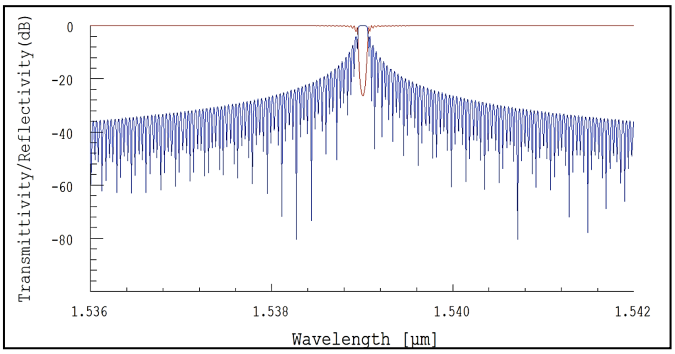

Fig. 10. Reflected (blue line) and transmitted spectrum (red line) of 1539.0067 nm FBG strain sensor

4.2. Experimental Results of Strain Sensing FBG

Both FBGs experience a shift in wavelength when weight is increased from 1 N to 10 N. Figure 11 shows a very minimal wavelength shift of 0.115 nm observed for the bare FBG. The strain that was applied from the experiment was then calculated using the formula from (2) and plotted in graph Fig. 12 between wavelength shifts. A clear correlation between weight applied and strain was observed as the higher the strain, the more the wavelength shift was detected.

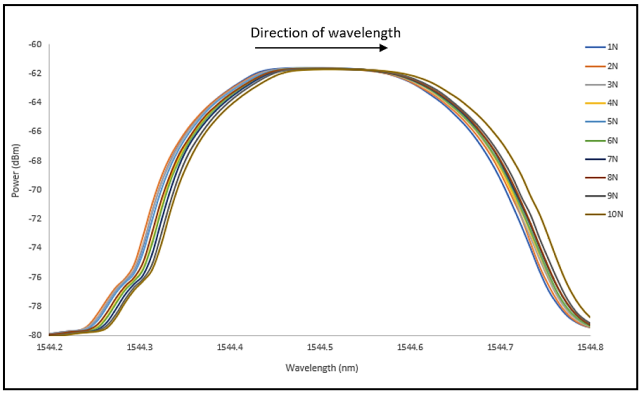

Fig.11. Reflected spectrum of bare FBG at different weight

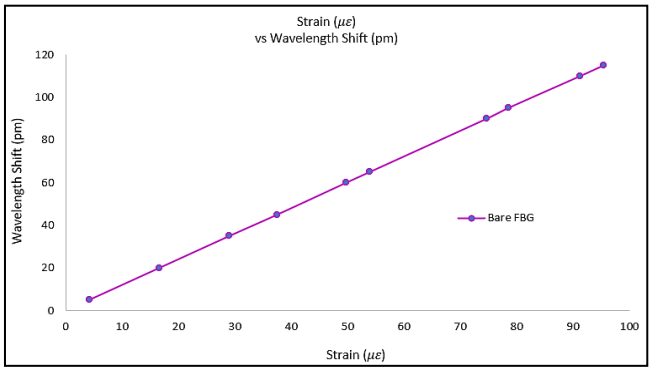

Fig. 12. Strain vs wavelength shift graph for bare FBG

As for the FBG strain sensor, the wavelength recorded at 10 N is 1539.3870 nm and the total wavelength shifted is 0.3803 nm which is slightly higher than the bare FBG due to the presence of the built-in strain sensor on the grating area of the FBG. The wavelength shift can be seen by viewing the zoom-in spectrum in Figure 13.

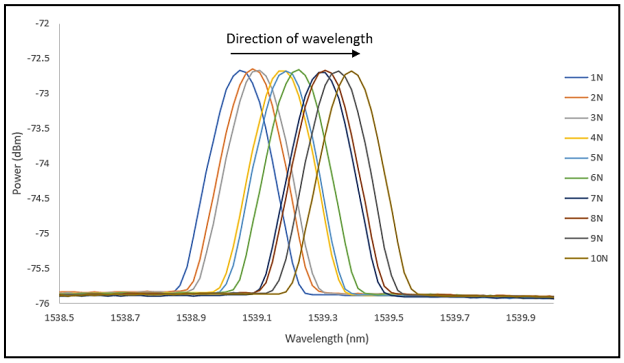

Fig. 13. Reflected spectrum of FBG strain sensor at different weight

The output wavelength shift for FBG strain sensor is then plotted as in Figure 14 which shows the spectral response of both FBGs towards the strain rises. A good linear correlation between the strain and wavelength shift can be observe in the graph below.

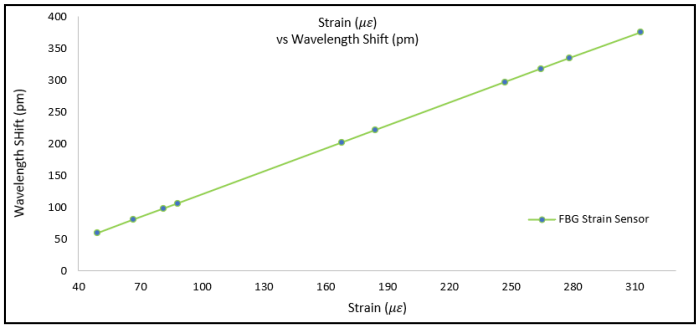

Fig. 14. Graph of strain versus wavelength shift of FBG strain sensor

Both fibers underwent increments in the Bragg wavelength value as formulated in the strain sensitivity equation (2) due to the strain dependence of refractive index and the thermal expansion as weight is increased up to 10 N. The equation demonstrates that the greater the weight applied, the higher the strain exerted, resulting in a greater wavelength shift.

The total wavelength shifted for both sensors can be used to determine which sensor is better. The Bragg wavelength changes measured for the bare and built-in FBG strain sensors between 1 N and 10 N are 0.1150 nm and 0.3803 nm, respectively. This indicates that both bare and FBG strain sensors can operate as strain sensors because their wavelengths shift as strain varies. However, the FBG strain sensor has a larger wavelength shift than the bare FBG, indicating that it has better sensor performance.

As the built-in strain sensor FBG produces a better result, demonstrating its possibilities for use in industrial commercial applications, particularly remote, real-time, high precision and early warning monitoring.

4.3. Comparison of Experimental and Simulation Result

The data gained from the simulation has been plotted in the figure Figure 15 to show the relationship between the strain applied and the wavelength shift. These outcomes demonstrate that simulation can be used to achieve different peak positions when the strain is applied to the grating period. Next, the results from both experimental and simulation are mapped in a linear graph as in Figure 16 so that it can be clearly compared.

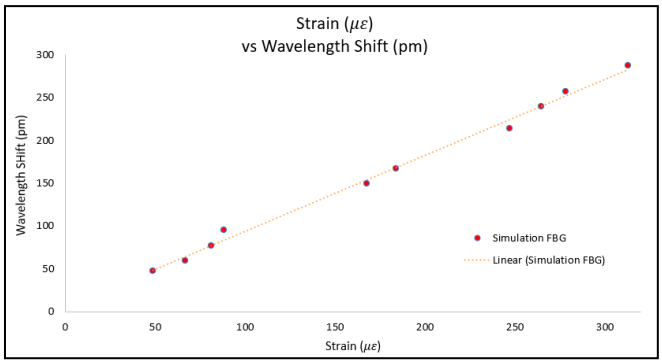

Fig. 15. Strain vs wavelength shift graph using simulation

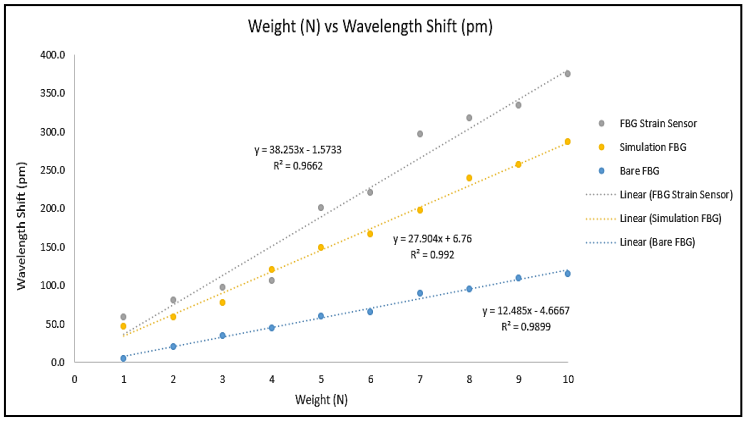

Fig.16. Comparison of simulation and experimental results of wavelength shift

According to Figure 16, the simulation's linearity is better than both experimental results, as the simulation software is only capable to simulate ideal strain sensor using uniform FBG. However, the experimental outcome for the built-in FBG sensor reveals that it is the best sensor as it has the highest strain sensitivity, indicating that real or physical testing outperforms simulation by 35%. The wavelength shift with respect to strain is applied, demonstrating the correlation of experimental data with the expected wavelength change in simulation. Consequently, the experimental results correlate well with simulation and confirm the proposed assumption for FBG as a strain sensor. Table 2 displays the clear comparison between results obtained.

Table 2
Performance of strain sensing experiment and simulation

Parameters	FBG strain sensor (experiment	Bare FBG (experiment)	Uniform FBG (simulation)
Sensitivity (pm/N)	38.25	12.49	27.91
Linearity (%)	96.62	98.99	99.20
Linear Range (N)	1 – 10	1 – 10	1 - 10
Total wavelength shift (pm)	380.30	115.00	287.30

The FBG strain sensor has a strain sensitivity of 38.35 pm/N, while the bare FBG has a strain sensitivity of 12.49 pm/N, signifying a more than two-fold improvement over the bare FBG. The improved strain sensitivity is owing to the fiber's built-in strain sensor, which makes it more sensitive to strain change. While the uniform FBG perform through simulation process resulting a better result from bare FBG in terms of linearity, sensitivity and wavelength shift in total.

5. Conclusions

In conclusion, the results and analysis for the FBG strain sensor is demonstrated in this paper. Both bare and FBG strain sensors are investigated experimentally to evaluate the strain sensitivity. Then, the uniform FBG is designed through simulation software, and it is proven that the wavelength of FBG sensors has a linear relationship with strain increase, which coincides with the applied weight. The strain sensitivity of the FBG strain sensor is 38.25 pm/N, which is higher than the strain sensitivity of the bare FBG (12.49 pm/N) and the uniform FBG (27.91 pm/N). The experimental results are more sensitive than the simulation results, which can be attributable to the simulation software's design parameters. The FBG strain sensor also demonstrates better resolution and wavelength shift compared to the other FBGs, proving its benefits as strain sensor.

Acknowledgement

The authors would like to thank Universiti Teknologi MARA (UiTM) for supporting this project under GPK research grant 600-RMC/GPK 5/3 (101/2020).

References

[1] Tao, L. I. A. O., P. E. I. Yifei, X. U. Jian, L. I. N. Heng, and N. I. N. G. Tigang. "Fiber Bragg grating temperature sensors applied in harsh environment of aerospace." In *Asia Communications and Photonics Conference*, pp. Su2A-20. Optica Publishing Group, 2018. https://doi.org/10.1109/acp.2018.8595842

[2] Aizzuddin, A. M., Z. M. Hafizi, L. V. Kee, E. Vorathin, and K. S. Lim. "Development of Fibre Bragg grating (FBG) dynamic pressure transducer with diminutive voltage inconsistency." In *IOP Conference Series: Materials Science and Engineering*, vol. 257, no. 1, p. 012080. IOP Publishing, 2017. https://doi.org/10.1088/1757-899x/257/1/012080

[3] Dante, Alex, Rodrigo Moreira Bacurau, Anderson Wedderhoff Spengler, Elnatan Chagas Ferreira, and José Antônio Siqueira Dias. "A temperature-independent interrogation technique for FBG sensors using monolithic multilayer piezoelectric actuators." *IEEE Transactions on instrumentation and measurement* 65, no. 11 (2016): 2476-2484. https://doi.org/10.1109/tim.2016.2594021

[4] More, Aniket Shivram, Pritam sanjay Lad, Shivram Ramnarayanan Krishnan, and Savita R. Bhosale. "Performance analysis of Strain sensor based on Fiber Bragg Grating." In *ITM Web of Conferences*, vol. 32, p. 02006. EDP Sciences, 2020. https://doi.org/10.1051/itmconf/20203202006

[5] Almubaied, Omar, Hwa Kian Chai, Md Rajibul Islam, Kok-Sing Lim, and Chee Ghuan Tan. "Monitoring corrosion process of reinforced concrete structure using FBG strain sensor." *IEEE Transactions on Instrumentation and Measurement* 66, no. 8 (2017): 2148-2155. https://doi.org/10.1109/tim.2017.2676218

[6] Liu, Hong-lin, Zheng-wei Zhu, Yong Zheng, Bang Liu, and Feng Xiao. "Experimental study on an FBG strain sensor." *Optical Fiber Technology* 40 (2018): 144-151. https://doi.org/10.1016/j.yofte.2017.09.003

[7] Wu, Hao, Qijing Lin, Zhuangde Jiang, Fuzheng Zhang, Lei Li, and Libo Zhao. "A temperature and strain sensor based on a cascade of double fiber Bragg grating." *Measurement Science and Technology* 30, no. 6 (2019): 065104. https://doi.org/10.1088/1361-6501/ab093e

[8] Tang, Zijuan, Shuqin Lou, Xin Wang, Wan Zhang, Shibo Yan, and Zhen Xing. "High-performance bending vector and strain sensor using a dual-tapered photonic crystal fiber Mach–Zehnder interferometer." *IEEE Sensors Journal* 19, no. 11 (2019): 4062-4068. https://doi.org/10.1109/jsen.2019.2895684

[9] Li, Ruiya, Yiyang Chen, Yuegang Tan, Zude Zhou, Tianliang Li, and Jian Mao. "Sensitivity enhancement of FBG-based strain sensor." *Sensors* 18, no. 5 (2018): 1607. https://doi.org/10.3390/s18051607

[10] Kachare, Nitin, and D. Sriram Kumar. "Analysis of simultaneous measurement of temperature and strain using different combinations of FBG." In *AIP Conference Proceedings*, vol. 1849, no. 1. AIP Publishing, 2017. https://doi.org/10.1063/1.4984178

[11] Razi, Muhammad Imaduddin Mohd, Mohd Rashidi Che Beson, Saidatul Norlyana Azemi, and Syed Alwee Aljunid. "FBG sensor strain performance analysis using optisystem software tools." *Indones J Electr Eng Comput Sci* 14, no. 2 (2019): 564-572. https://doi.org/10.11591/ijeecs.v14.i2.pp564-572

[12] Tahhan, Shaymaa R., Mudhafar Hussein Ali, Marwah Ali Zaidan Al-Ogaidi, and Abdulla Khudiar Abass. "Impact of Apodization Profile on Performance of Fiber Bragg Grating Strain-Temperature Sensor." *J. Commun.* 14, no. 1 (2019): 53-57. https://doi.org/10.12720/jcm.14.1.53-57

[13] Kumar, Jayant, and Devendra Chack. "FBG based strain sensor with temperature compensation for structural health monitoring." In *2018 4th International Conference on Recent Advances in Information Technology (RAIT)*, pp. 1-4. IEEE, 2018. https://doi.org/10.1109/rait.2018.8388987

[14] Elgaud, M. M., Mohd Saiful Dzulkefly Zan, A. A. G. Abushagur, and A. Ashrif A. Bakar. "Analysis of independent strain-temperature fiber Bragg grating sensing technique using OptiSystem and OptiGrating." In *2016 IEEE 6th International Conference on Photonics (ICP)*, pp. 1-3. IEEE, 2016. https://doi.org/10.1109/icp.2016.7510036

[15] Guo, Jun-Yi, Jin-Hui Fang, Bin Shi, Cheng-Cheng Zhang, and Liang Liu. "High-sensitivity water leakage detection and localization in tunnels using novel ultra-weak fiber Bragg grating sensing technology." *Tunnelling and Underground Space Technology* 144 (2024): 105574. https://doi.org/10.1016/j.tust.2023.105574

[16] Huang, Hong-wei, Qing-tong Li, and Dong-ming Zhang. "Deep learning based image recognition for crack and leakage defects of metro shield tunnel." *Tunnelling and underground space technology* 77 (2018): 166-176. https://doi.org/10.1016/j.tust.2018.04.002

[17] Li, Diyuan, Xibing Li, Charlie C. Li, Bingren Huang, Fengqiang Gong, and Wei Zhang. "Case studies of groundwater flow into tunnels and an innovative water-gathering system for water drainage." *Tunnelling and Underground Space Technology* 24, no. 3 (2009): 260-268. https://doi.org/10.1016/j.tust.2008.08.006

[18] Yuan, Yong, Xiaomo Jiang, and Xian Liu. "Predictive maintenance of shield tunnels." *Tunnelling and Underground Space Technology* 38 (2013): 69-86. https://doi.org/10.1016/j.tust.2013.05.004

[19] Wongsaroj, J., K. Soga, and R. J. Mair. "Tunnelling-induced consolidation settlements in London Clay." *Géotechnique* 63, no. 13 (2013): 1103-1115. https://doi.org/10.1680/geot.12.P.126

[20] Yu, Chao, Annan Zhou, Jun Chen, Arul Arulrajah, and Suksun Horpibulsuk. "Analysis of a tunnel failure caused by leakage of the shield tail seal system." *Underground Space* 5, no. 2 (2020): 105-114. https://doi.org/10.1016/j.undsp.2018.11.003